# Relative *g*-factor measurements in the stable Te isotopes

Andrew E. Stuchbery,[1] Akiumi Nakamura,[1] Anna N. Wilson,[1,2] Paul M. Davidson,[1] Hiroshi Watanabe,[1] and Alexander I. Levon[3]

[1]*Department of Nuclear Physics, Australian National University, Canberra ACT 0200, Australia*
[2]*Department of Physics, Australian National University, Canberra ACT 0200, Australia*
[3]*Institute for Nuclear Research, Prospekt Nauki 47, 03680 Kiev, Ukraine*

(Received 12 February 2007; published 6 September 2007)

The $g(2_1^+)$ values in the even Te isotopes between $^{122}$Te and $^{130}$Te have been measured simultaneously, relative to each other, by the transient-field technique. In addition, $g$ factors were also measured for the $3/2_2^+$ and $5/2_1^+$ levels in $^{125}$Te.

DOI: 10.1103/PhysRevC.76.034306 PACS number(s): 21.10.Ky, 25.70.De, 27.60.+j

## I. INTRODUCTION

The availability of radioactive beams is affording new opportunities to study the structure of nuclei near $^{132}_{50}Sn_{82}$ and unveil new aspects of nuclear structure. Attention has recently been given to Coulomb excitation of the neutron-rich Te isotopes [1,2]. An anomalously low value reported for the $B(E2; 0_1^+ \rightarrow 2_1^+)$ in $^{136}_{52}Te_{84}$ [1] has attracted much theoretical attention [3–5]. The small $B(E2)$ value was interpreted [1] as evidence for a predominantly neutron excitation, a suggestion that is supported by some theories [3,4], but not by others [5]. Experimental $g$ factors in the nearby stable Xe isotopes, which have a similar number of valence nucleons, have revealed a combination of single-particle and collective features in the low-excitation states [6].

It is clear that a $g$-factor measurement on $^{136}$Te would prove most enlightening. The feasibility of such a measurement has been demonstrated recently by the work of Stone and coworkers [7], who used the recoil in vacuum (RIV) technique to measure the $g$ factor of the first-excited state of $^{132}$Te produced as a radioactive beam. At present the accuracy of the RIV technique for the Te isotopes is limited to a significant degree by uncertainties in the $g$ factors of the stable isotopes $^{122}$Te, $^{126}$Te, and $^{130}$Te, which must be used for calibration. There are two problems concerning the previous $g$-factor data for these isotopes to be addressed in the present work: First, one transient-field measurement [8] reported a small $g$ factor in $^{126}$Te, which was not confirmed in other measurements [9, 10]. Second, the existing measurements on $^{130}$Te are not very precise [11]. The primary experimental purpose here is to measure the ratio of $g$ factors in $^{130}$Te and $^{126}$Te with high precision. To this end, a simultaneous relative measurement of the $g$ factors in the even-even isotopes between $^{122}$Te and $^{130}$Te has been performed using the transient-field technique and a natural target. As a byproduct, the $g$ factors were also measured for the $3/2_2^+$ and $5/2_1^+$ levels in $^{125}$Te.

Historically, there have been many measurements of the electric quadrupole moments [12–17] and magnetic dipole moments [8–10,18–26] of the first $2^+$ states in the stable even-even Te isotopes. These isotopes show a transition from structures that are amenable to shell model calculations near $N = 82$ toward collective vibrational-like structures in the more neutron-deficient isotopes. The early measurements of the spectroscopic quadrupole moments, by the reorientation effect in Coulomb excitation, were motivated by a confrontation between the simple vibrational picture and experimental quadrupole moments that were clearly nonzero. Many magnetic moment measurements have also been performed. A number of these measurements were triggered by the observation of anomalously large $g(2_1^+)$ values ($\gg Z/A$) in an implantation perturbed angular correlation (IMPAC) study [18]. The discovery of the transient field followed from these observations—the large observed precessions were not due to the magnitude of the nuclear $g$ factors, but to the presence of a large 'transient' hyperfine field which acts on ions moving swiftly within a ferromagnet [27].

The present paper is arranged as follows. Section II reports the transient-field measurements (Experimental Procedures and Analysis). The emphasis is on the even isotopes. Results for the $2_1^+$ states in the even isotopes are given in Sec. III. The calibration of the transient field, which is required to obtain absolute $g$ factors, is discussed in Sec. IV. This section also compares the present $g$ factors with previously reported values. Results for $^{125}$Te are given in Sec. V. A summary and concluding remarks follow (Sec. VI).

An accompanying paper [28] will consider the implications of the present $g$ factor results for the modeling and calibration of the RIV interaction, and hence for radioactive-beam $g$ factor measurements by the RIV technique.

## II. TRANSIENT FIELD *g*-FACTOR MEASUREMENTS

### A. Experimental procedures

Gyromagnetic ratios of the $2_1^+$ states in the even isotopes between $^{122}$Te and $^{130}$Te were measured simultaneously, relative to each other, by the transient-field technique. Although not optimized for the odd-$A$ nucleus $^{125}$Te, the $g$ factors of its $3/2_2^+$ and $5/2_1^+$ states at 444 keV and 464 keV, respectively, were also measured. The experimental procedures were similar to those in previous work [29–32]. Schematic views of the apparatus are shown in Fig. 1. States of interest were Coulomb excited using beams of 195 MeV $^{58}$Ni from the ANU 14UD Pelletron accelerator. The target was composed of $^{nat}$Te, 1 mg/cm$^2$ thick, evaporated onto an annealed iron foil 4.9 mg/cm$^2$

 

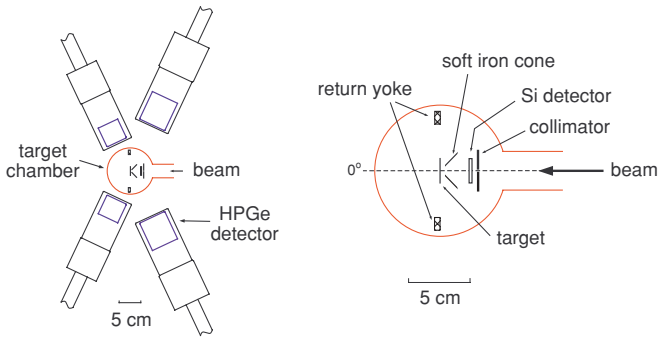


FIG. 1. (Color online) Left: Plan view of the target chamber and $\gamma$-ray detectors. Right: Plan view of components inside the target chamber.

thick. Te nuclei recoiled through the iron foil, where they experienced the transient field, and stopped in a nonmagnetic backing layer of copper 4.5 mg/cm$^2$ thick, evaporated on the back of the iron foil. For additional mechanical support and improved thermal contact with a liquid-nitrogen cooled target mount, the multilayered target was pressed onto thicker ($\sim$12 $\mu$m) copper foil using an evaporated layer of indium as adhesive. Throughout the measurements the target temperature was maintained at $\approx$90 K ($-183^\circ$C) to reduce the effects of beam heating, and to help minimize the loss of Te (melting point 450°C) from the target. The iron foils were polarized perpendicular to the $\gamma$-ray detection plane by a small electromagnet, which produced a field of 0.08 T, which is more than sufficient to saturate a well annealed iron foil [33]. The direction of the polarizing field was reversed automatically, approximately every 15 min. Backscattered $^{58}$Ni ions were detected in two rectangular silicon detectors 9.2 mm wide by 10.2 mm high placed 23.7 mm from the target, 3.85 mm above and below the beam axis (see Fig. 2). The average scattering angle was 159°.

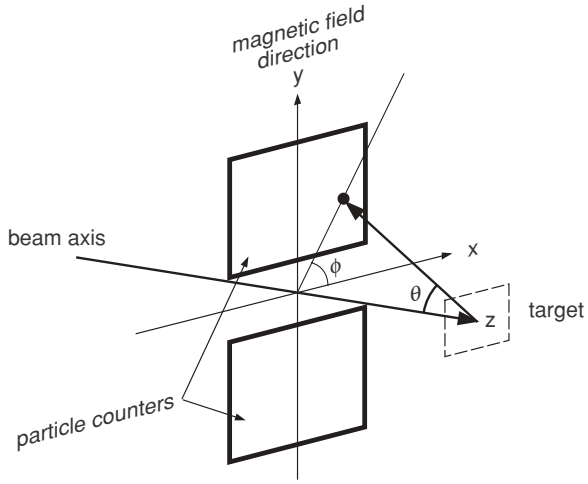


FIG. 2. Schematic of particle detectors defining the coordinate frame used for the angular correlation calculations. The beam is along the $z$-axis and the magnetic field direction is along the $y$-axis. The $\gamma$-ray detectors are in the $xz$-plane.

The precessions of the nuclei due to the transient-field interaction were measured by placing pairs of Ge detectors in the forward and backward quadrants where the particle-$\gamma$ angular correlations for $E2$ transitions have near maximal slope and hence give near-optimum sensitivity to the nuclear precession.

Two similar runs were performed. To improve the count rate in the second run, the beam current was increased from 1.5 pnA to 7.7 pnA, and one pair of $\gamma$-ray detectors was repositioned. In both runs the forward detectors (efficiency $\sim$20%) were placed at $\pm 65^\circ$ to the beam axis and such that the detector crystals subtended a half angle of 20°. The backward $\gamma$-ray detectors (efficiency $\sim$50%) were placed at $\pm 120^\circ$, subtending 11.4° during the first run. They were then moved to $\pm 115^\circ$, subtending 15.2°, for the second run; this case is illustrated in Fig. 1.

### B. Analysis

Experimental precession angles, $\Delta\Theta$, were determined by standard procedures [6,8,29,31,34]. The double ratio $\rho$ was formed for each pair of $\gamma$-ray detectors:

$$\rho = \sqrt{\frac{N(+\theta_\gamma)\uparrow}{N(+\theta_\gamma)\downarrow}\frac{N(-\theta_\gamma)\downarrow}{N(-\theta_\gamma)\uparrow}}, \tag{1}$$

where $N(\pm\theta_\gamma)\uparrow\downarrow$ denote the counting rates at $\pm\theta_\gamma$ for field up($\uparrow$) and down($\downarrow$). The precession angles were then determined from

$$\Delta\Theta = \frac{\epsilon}{S}, \tag{2}$$

where $\epsilon = (1-\rho)/(1+\rho)$ and $S$ is the logarithmic derivative of the angular correlation, $W(\theta)$, evaluated at the detection angle $\theta_\gamma$. Specifically,

$$S = \frac{1}{W(\theta)}\frac{dW}{d\theta}\bigg|_{\theta_\gamma}. \tag{3}$$

The required angular correlations were calculated in the present work. They are similar for all of the even Te isotopes and for simultaneous relative measurements the (relative) $2_1^+ \rightarrow 0_1^+$ particle-$\gamma$ angular correlations can be calculated more accurately than they can be measured. This statement is backed up by numerous measurements and calculations of angular correlations by our group over the past few decades [29–32,35–49]. It is particularly relevant to note that angular correlations have been measured and calculated in several sequences of transitional nuclei such as $^{92-100}$Mo [49], $^{154-160}$Gd [35,38,47], $^{182-186}$W [36,39,43], $^{188-192}$Os [29,41,43], and $^{190-198}$Pt [39,43–46] where the changes in nuclear structure cause changes in feeding patterns that are at least as pronounced as in the present study of $^{122-130}$Te.

The formalism for the calculation of these angular correlations is straight forward, but complicated somewhat by the use of rectangular particle detectors, which break the symmetry about the beam axis [35]. The required theoretical expression for the angular correlation after Coulomb excitation

(see Refs. [50,51] and references therein) can be written as

$$W(\theta_\gamma) = \sum_{k,q} B_{kq}(\theta,\phi) F_k Q_k D^{k*}_{q0}(0,\theta_\gamma,0), \tag{4}$$

where $B_{kq}(\theta,\phi)$ is the statistical tensor, which defines the spin alignment of the initial state, and which depends on the particle scattering angles $(\theta,\phi)$ and the geometry of the particle detector. $F_k$ represents the usual $F$-coefficient for the $\gamma$-ray transition [52], $Q_k$ is the attenuation factor for the finite size of the $\gamma$-ray detector, and $D^k_{q0}(0,\theta_\gamma,0)$ is the rotation matrix, which depends on the $\gamma$-ray detection angle $\theta_\gamma$. In the applications of interest $k = 0, 2, 4$. The coordinate frame is right-handed with the beam along the positive $z$-axis as shown in Fig. 2. Since the magnetic field is along the $y$ axis and the $\gamma$-ray detectors are in the $xz$ plane, the rotation matrix is equivalent to an associated Legendre polynomial.

Evaluation of the angular correlation requires the calculation of the statistical tensor using the de Boer-Winther code [53]. In this code the statistical tensors $\rho_{kq'}(\theta,0)$ correspond to the particle-scattering plane. To calculate the angular correlations applicable for the experiments requires the tensors corresponding to scattering at angle $\phi$ as defined in Fig. 2. These are given by

$$\rho_{kq}(\theta,\phi) = \sum_{q'} \rho_{kq'}(\theta,0) D^k_{q'q}(\phi,0,0) \tag{5}$$

$$= \rho_{kq}(\theta,0) e^{iq\phi}. \tag{6}$$

Thus the required average statistical tensor at a given beam energy is given by

$$\langle \rho_{kq} \rangle = \frac{\int_\theta \int_\phi \rho_{kq}(\theta,0) e^{iq\phi} \frac{d\sigma}{d\Omega} d\Omega}{\int_\theta \int_\phi \frac{d\sigma}{d\Omega} d\Omega}, \tag{7}$$

where the integrals are over the dimensions of the particle detector and $\frac{d\sigma}{d\Omega}$ is the cross section for Coulomb excitation corresponding to the scattering angle $\theta$. In the geometry used here (Fig. 2) there are two particle detectors placed symmetrically about the beam axis such that the numerical integration can be limited to the positive quadrant, $0^\circ \leqslant \phi \leqslant 90^\circ$. The factor $e^{iq\phi}$ can then be replaced by $(e^{iq\phi} + e^{-iq\phi} + e^{iq(\phi+\pi)} + e^{-iq(\phi+\pi)})/4$, which is $\cos q\phi$ if $q$ is even and zero if $q$ is odd.

To obtain the statistical tensors of direct relevance to the present experiments, a further integration was performed to average over the energy loss of the beam in the target. Corrections for feeding from higher states were also made (see below). The statistical tensors required in Eq. (4), $B_{kq}$, are related to those from the Coulomb excitation calculation, $\rho_{kq}(\theta,\phi)$, by $B_{kq}(\theta,\phi) = \sqrt{(2k+1)}\rho_{kq}(\theta,\phi)$. For an annular counter only the $q = 0$ tensors are non zero. The broken azimuthal symmetry gives rise to finite $\langle B_{kq} \rangle$ values for $q \neq 0$, however these terms are small in the present case because the scattering angle remains near $180^\circ$ and the spin of the excited state is aligned predominantly in the plane perpendicular to the beam. The $q \neq 0$ terms change $S(65^\circ)$ for $^{126}$Te by about 3.5%.

The Coulomb excitation calculations employed $E2$ matrix elements from the literature [12–17]. Along with the $0^+_1$ ground state and first excited state, $2^+_1$, the calculations for $^{124}$Te through $^{130}$Te included the weakly populated $4^+_1$ and $2^+_2$ states. As in the quadrupole moment studies [12–17], the calculation for $^{122}$Te included the $0^+_2$ and $2^+_3$ states in addition to the $0^+_1$, $2^+_1$, $4^+_1$, and $2^+_2$ states. There is some variation in the reported matrix elements for the weakly populated higher-excited states. However the uncertainties in these matrix elements are not important for the angular correlation calculation because (i) the statistical tensors depend mainly on the reaction geometry and are largely independent of the matrix elements, and (ii) the feeding contribution to the alignment of the $2^+_1$ state, which depends on the uncertain matrix elements, is relatively small.

### C. Formalism for feeding corrections

As noted above, there is a contribution due to feeding from higher-excited states in both the unperturbed and perturbed angular correlations of the $2^+_1 \rightarrow 0^+_1$ $\gamma$ ray. Although relatively small, this contribution increases systematically from $^{130}$Te to $^{122}$Te as the collectivity increases. Detailed general descriptions of the formalism for feeding corrections in transient-field $g$-factor measurements have been given in previous work, e.g., Refs. [29–31]. A simplified formalism to convey the features of relevance to the present measurements is given here. It is helpful to begin by reviewing the effect of feeding on the unperturbed angular correlation. In the present Coulomb-excitation study of the even Te isotopes, the weakly populated higher-excited states, $0^+_2$, $2^+_2$, $2^+_3$, and $4^+_1$, all decay to the $2^+_1$ states via a single $\gamma$-ray transition. The observed (fed) unperturbed angular correlation can thus be evaluated by replacing the statistical tensor $B_{kq}(2^+_1)$ in Eq. (4) by $\langle B_{kq}(2^+_1) \rangle_{\rm fed}$, which is defined as

$$\langle B_{kq}(2^+_1) \rangle_{\rm fed} = \frac{N^0_{2^+_1} B_{kq}(2^+_1) + \sum_{i>2^+_1} N^0_i B_{kq}(i) U_k(i \rightarrow 2^+_1)}{N^0_{2^+_1} + \sum_{i>2^+_1} N^0_i}, \tag{8}$$

where $N^0_{2^+_1}$ is the direct population of the $2^+_1$ state and $N^0_i$ is the population of the $2^+_1$ state due to feeding from the higher-excited state $i$. ($N^0_{2^+_1}$ is proportional to the cross section for exciting the $2^+_1$ state; $N^0_i$ is proportional to the cross section for exciting the state $i$ and to the branching ratio for the $i \rightarrow 2^+_1$ decay.) $U_k(i \rightarrow 2^+_1)$ is the well-known deorientation coefficient [52] for the $i \rightarrow 2^+_1$ decay, which may depend on the mixing ratio of the $i \rightarrow 2^+_1$ transition.

The analysis of the precession data begins with an analysis of the observed (i.e., fed) unperturbed and perturbed angular correlations using Eqs. (1)–(3). Thus the observed precession angle, including feeding, is given by Eq. (2), which may be written as

$$\Delta\Theta_{\rm obs} = \epsilon_{\rm obs}/S_{\rm fed}, \tag{9}$$

where $S_{\rm fed}$ is evaluated for the fed angular correlation by substitution of $\langle B_{kq}(2^+_1) \rangle_{\rm fed}$ into Eq. (4). In the case where the lifetimes of all states are much greater than the transit time of the ions through the ferromagnetic foil ($t_{\rm Fe}$), $\Delta\Theta_{\rm obs}$ can be

TABLE I. Summary of measured precession angles in the even Te isotopes.

| Isotope | $E_\gamma$ (keV) | $\epsilon(\pm 65^\circ)$ ($\times 10^3$) | $S(65^\circ)$ | $\epsilon(\pm 120^\circ)$ ($\times 10^3$) | $S(120^\circ)$ | $\epsilon(\pm 115^\circ)$ ($\times 10^3$) | $S(115^\circ)$ | $\langle \Delta\Theta \rangle$ (mrad) |
|---|---|---|---|---|---|---|---|---|
| $^{122}$Te | 564 | 52.3(10.0) | −2.54 | −80.7(14.6) | 2.01 | −48.9(14.3) | 2.69 | −23.01(2.90) |
| $^{124}$Te | 603 | 61.2(7.0) | −2.57 | −56.8(10.2) | 2.03 | −57.9(9.8) | 2.72 | −23.68(1.99) |
| $^{126}$Te | 666 | 61.3(3.5) | −2.62 | −44.5(5.2) | 2.06 | −51.7(5.0) | 2.77 | −21.69(0.99) |
| $^{128}$Te | 743 | 57.1(3.2) | −2.68 | −41.6(4.6) | 2.10 | −52.6(4.4) | 2.84 | −20.19(0.87) |
| $^{130}$Te | 839 | 65.0(4.0) | −2.77 | −46.6(5.8) | 2.16 | −64.2(5.5) | 2.93 | −22.66(1.05) |

related to the precessions of the individual levels as

$$\Delta\Theta_{\rm obs} = \frac{N^0_{2^+_1}\frac{dW_{20}}{d\theta}\Delta\Theta_{2^+_1} + \sum_{i>2^+_1} N^0_i \frac{dW_{i20}}{d\theta}\Delta\Theta_i}{N^0_{2^+_1}\frac{dW_{20}}{d\theta} + \sum_{i>2^+_1} N^0_i \frac{dW_{i20}}{d\theta}}, \quad (10)$$

where $\Delta\Theta_i$ is the precession of the level $i$, $W_{20}$ is the angular correlation of the $2^+_1 \rightarrow 0^+_1$ transition due to direct population of the $2^+_1$ state and $W_{i20}$ is the angular correlation of the $2^+_1 \rightarrow 0^+_1$ transition due to feeding from level $i$.

It is helpful to rewrite Eq. (10) as

$$\Delta\Theta_{\rm obs} = \sum_{j \geqslant 2^+_1} A_j \Delta\Theta_j, \quad (11)$$

where the sum now includes the contribution associated with the direct population of the $2^+_1$ state. It will become apparent below that in the present work $A_{2^+_1} \gg A_{j\neq 2^+_1}$.

In collective nuclei, whether vibrational or rotational, the $g$ factors of the low-excitation states are essentially identical. In such cases $\Delta\Theta_{\rm obs} = \Delta\Theta_{2^+_1} = \Delta\Theta_i$. Since the $g$ factors of the higher-excited states in the Te isotopes are unknown, they were assumed to be identical to that of the $2^+_1$ state for the evaluation of feeding corrections. The uncertainty in the $g(2^+_1)$ values due to this assumption is evaluated below.

## III. EXPERIMENTAL RESULTS: $2^+$ STATES

This section focuses on results for the $2^+$ states in the even isotopes; results for $^{125}$Te are reported in Sec. V.

Figure 3 shows an example of a $\gamma$-ray spectrum and Table I gives the results of the precession measurements. Details of the reaction kinematics are given in Table II. This table also includes an estimate of the transient-field precession per unit $g$ factor, which is given by

$$\phi(\tau) = \Delta\Theta/g = -\frac{\mu_N}{\hbar}\int_{T_i}^{T_e} B_{\rm tr}(t) e^{-t/\tau} dt, \quad (12)$$

where $g$ is the nuclear $g$ factor, $\tau$ the lifetime of the nuclear state, $B_{\rm tr}$ is the transient-field strength, and $T_i$ and $T_e$ are the times, after excitation at $t = 0$, at which the ion enters into and exits from the iron foil. For the estimates in Table II, the transient field was assumed to follow the velocity dependence of Rutgers parametrization [55], with the overall strength scaled to match the field calibration adopted below. Since the Te isotopes have a very similar velocity range and transit time for their passage through the iron host, the *relative* $\phi$ values in Table II are very insensitive to the choice of transient-field parametrization.

As is evident from the Doppler broadened high-energy tails on the peaks in Fig. 3, a small fraction of the excited nuclei decay whilst in transit through the iron layer of the target. The exponential factor in Eq. (12) takes account of these decays in flight. If the whole lineshape is integrated to evaluate the double ratio $\rho$, Eq. (1), the observed precessions must be corrected by multiplying by $\phi(\infty)/\phi(\tau)$ [see Eq. (12)] if the relative precessions are to reflect relative $g$ factors. Alternatively, the effect of different lifetimes may be side-stepped in the analysis of the $g$ factors by integrating only the stopped part of the relevant $\gamma$-ray peak (i.e., omitting the Doppler tail). This latter procedure can be justified by Monte Carlo simulations of the $\gamma$-ray lineshape, along the lines of the calculations in [56]. Both methods of analysis were performed and checked for consistency, however since there can be contaminant peaks under the Doppler tail, the results of the second approach are adopted here.

It can be seen from the calculated precession angles in the final column of Table II that there is a systematic increase in

TABLE II. Kinematics for Te recoiling in iron. $\tau(2^+_1)$ is the mean life of the $2^+_1$ level. $\langle E_i \rangle$ and $\langle E_e \rangle$ are the average energies with which the Te ions enter into and exit from the iron foil. The corresponding ion velocities are $\langle v_i/v_0 \rangle$ and $\langle v_e/v_0 \rangle$. The average ion velocity is $\langle v/v_0 \rangle$. $v_0 = c/137$ is the Bohr velocity. These quantities were calculated with the stopping powers of Ziegler *et al.* [54]. $\phi$ is the transient-field precession per unit $g$ factor calculated as described in the text.

| Isotope | $\tau(2^+_1)$ (ps) | $\langle E_i \rangle$ (MeV) | $\langle E_e \rangle$ (MeV) | $\langle v_i/v_0 \rangle$ | $\langle v_e/v_0 \rangle$ | $\langle v/v_0 \rangle$ | $t_{\rm Fe}$ (fs) | $-\phi(\tau)$ (mrad) | $-\phi(\infty)$ (mrad) |
|---|---|---|---|---|---|---|---|---|---|
| $^{122}$Te | 10.8 | 147.7 | 15.4 | 6.98 | 2.26 | 4.03 | 711 | 61.1 | 63.2 |
| $^{124}$Te | 9.0 | 146.7 | 15.1 | 6.90 | 2.22 | 4.00 | 716 | 60.9 | 63.4 |
| $^{126}$Te | 6.5 | 145.6 | 14.8 | 6.82 | 2.18 | 3.97 | 721 | 60.1 | 63.7 |
| $^{128}$Te | 4.7 | 144.6 | 14.5 | 6.75 | 2.14 | 3.95 | 726 | 59.0 | 63.9 |
| $^{130}$Te | 3.3 | 143.5 | 14.3 | 6.67 | 2.11 | 3.92 | 731 | 57.2 | 64.2 |

TABLE III. Parameters for feeding corrections to $2_1^+$-state precessions.

| Isotope | Level $j$ | $N_j^0$ | $\frac{dW_{j20}}{d\theta}$ | $A_j$ |
|---|---|---|---|---|
| $^{122}$Te | $2_1^+$ | 81.5 | 3.05 | 0.948 |
| | $4_1^+$ | 11.4 | 1.04 | 0.045 |
| | $2_2^+$ | 5.0 | 0.36 | 0.007 |
| | $0_2^+$ | 1.8 | 0 | 0 |
| | $2_3^+$ | 0.09 | −0.31 | 0 |
| $^{126}$Te | $2_1^+$ | 85.8 | 3.05 | 0.960 |
| | $4_1^+$ | 8.5 | 1.04 | 0.032 |
| | $2_2^+$ | 5.7 | 0.40 | 0.008 |
| $^{130}$Te | $2_1^+$ | 93.6 | 3.04 | 0.988 |
| | $4_1^+$ | 4.4 | 1.04 | 0.159 |
| | $2_2^+$ | 2.0 | −0.65 | −0.005 |

$\phi(\infty)$ with mass due to the increasing transit times through the iron foil, $t_{Fe}$. This change in $\phi(\infty)$ with mass has been corrected for in the analysis of the $g$ factors, although it is much smaller than the statistical uncertainties in the measured precession angles.

The effects of feeding into the $2_1^+$ states from Coulomb-excited states with $I > 2$ will now be discussed by reference to the parameters for $^{122}$Te, $^{126}$Te, and $^{130}$Te shown in Table III. Feeding intensities increase from ∼6% of the total intensity in the $2_1^+ \rightarrow 0_1^+$ transition in $^{130}$Te, to ∼18% in $^{122}$Te as the collectivity increases from $^{130}$Te to $^{122}$Te. [See the $N^0$ values in Table III and the discussion of Eq. (10).]

As noted above, the $g(2_1^+)$ values were determined by assuming that, in each nucleus, the $g$ factors of the higher-excited states are the same as the $g$ factor of the first-excited state. This assumption of equal $g$ factors may not be correct, especially for $^{130}$Te. Shell model calculations predict $g(4_1^+)/g(2_1^+) \sim 1.3$ in $^{130}$Te [6] and $g(4_1^+)/g(2_1^+) \sim 1.6$ in $^{132}$Te [5,6]. Similar $g$-factor ratios were are predicted [6] for the isotones $^{132}$Xe and $^{134}$Xe, where the experimental $g(4_1^+)/g(2_1^+)$ ratios are $1.94 \pm 0.36$ and $2.34 \pm 0.40$, respectively [6]. A quantitative analysis was therefore performed to evaluate the

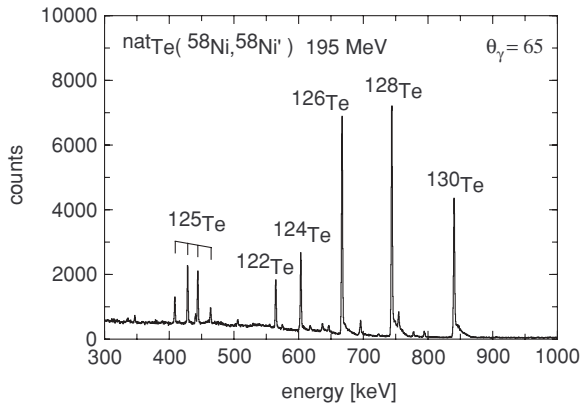


FIG. 3. Gamma-ray spectrum for the detector at +65° to the beam. This spectrum represents ∼55% of the data taken for 'field up.'

TABLE IV. Present $g$-factor results.

| Isotope | $-\langle\Delta\Theta\rangle$ (mrad) | | $g$ factor |
|---|---|---|---|
| | observed | corrected[a] | |
| $^{122}$Te | 23.01(2.90) | 23.01(2.94) | +0.361(46) |
| $^{124}$Te | 23.68(1.99) | 23.60(2.04) | +0.371(32) |
| $^{126}$Te | 21.69(0.99) | 21.53(1.07) | +0.338(17) |
| $^{128}$Te | 20.19(0.87) | 19.97(0.95) | +0.314(15) |
| $^{130}$Te | 22.66(1.05) | 22.32(1.12) | +0.351(18) |

[a]Corrected for the mass-dependence of the transient-field precession due to small differences in kinematic conditions. Errors include the uncertainty in feeding contributions. See text.

effect on the observed precession angle for $^{130}$Te, should the $g$ factors of the higher states not be identical to that of the $2_1^+$ state. The formalism for this analysis has been given in Sec. II C and the relevant parameters are summarized in Table III. It was found that for $^{130}$Te $\Delta\Theta_{obs}$ is essentially independent of $g(2_2^+)$, changing by $\sim \pm 0.1$ mrad (or $< \pm 0.5\%$) for $0 < g(2_2^+) < 2g(2_1^+)$. When $g(4_1^+)$ varies through the same range, the observed precession $\Delta\Theta_{obs}$ changes by $\pm 0.4$ mrad (or $\pm 1.7\%$). As the intensity of the feeding contribution to the observed precession for the $2_1^+$ state increases with increasing collectivity, from $^{130}$Te to $^{122}$Te, so does it become a more sound assumption that $g(2_1^+) = g(2_2^+) = g(4_1^+)$. Furthermore, it can be seen from Table III that the measured precessions are insensitive to the precessions of the higher-lying states in all cases because the values of the coefficients $A_j$ in Eq. (11) are very much larger for the $2_1^+$ states than for the higher states.

Based on these considerations, the uncertainties assigned to the extracted $g$ factors include an uncertainty of $\pm 2\%$ added in quadrature, to cover uncertainties in the effect of feeding. Table IV shows the observed and corrected precession angles, and the extracted $g$ factors. Note that the relative $g$ factor values in the final column of Table IV are independent of the transient-field calibration.

## IV. TRANSIENT FIELD CALIBRATION AND COMPARISONS WITH PREVIOUS $g$-FACTOR MEASUREMENTS

There have been several previous measurements of the $2_1^+$-state $g$ factors in the even Te isotopes. These include several radioactivity measurements on $^{122}$Te and $^{124}$Te [19–24] by the integral perturbed angular correlation (IPAC) technique, thick-foil implantation perturbed angular correlation (IMPAC) studies [18,25–27], and three previous measurements using the transient-field technique [8–10].

It has been shown that the static hyperfine magnetic fields for iron hosts measured in-beam by the IMPAC technique are quenched for about 6 ps by the violence of the implantation process [57]. Since the lifetimes of the $2_1^+$ states in the Te isotopes range from ∼3 ps to ∼11 ps, the presence of this preequilibrium disruption of the hyperfine field, which lasts for several picoseconds, makes it impossible to obtain reliable $g$-factor values from the IMPAC measurements on these isotopes.

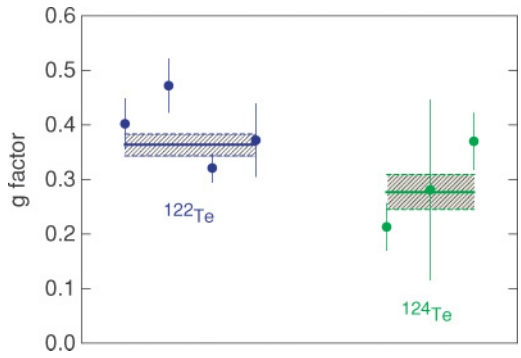


FIG. 4. (Color online) Integral perturbed angular correlation measurements of $2_1^+$-state $g$ factors in $^{122}$Te and $^{124}$Te obtained by the radioactivity technique in which $^{122}$Sb and $^{124}$Sb sources were dissolved in iron hosts [19–24].

The thick-foil IMPAC measurements [18,25–27] are therefore excluded from the present discussion.

The results of the (off-line) radioactivity measurements, which do not suffer from the in-beam preequilibrium effects noted above, are summarized in Fig. 4. These results have been reevaluated to correspond to the $2_1^+$ level lifetimes adopted by Raman *et al.* [58]. The weighted average of the results, and its error range, are indicated by the shaded bands in Fig. 4. Although there is some scatter, the individual results in Fig. 4 are reasonably consistent with the relevant average value, and, as will be seen below, the ratio of $g$ factors in $^{122}$Te and $^{124}$Te is reasonably consistent with the subsequent independent measurements.

A number of procedures have been proposed for evaluating the 'correct' average values from a potentially discrepant data set. Several of these procedures have been discussed by Rajput and MacMahon [59]. Unfortunately the different methods can give different values for both the average and its assigned error, so the choice of one procedure over another remains somewhat subjective. In view of this subjectivity, and for additional reasons to be outlined below, the present work adopts the conventional weighted average and its error for the radioactivity measurements. However the averaging of the data was examined further: The radioactivity data for $^{122}$Te and $^{124}$Te were also averaged using the limitation of relative statistical weight (LSW), the normalized residual method (NRM), and the Rajeval technique (RT) [59]. It was found that whereas the LSW method gives the same average value as the conventional weighted average, the other techniques (NRM and RT) propose somewhat different values for the average $g$ factors in $^{122}$Te and $^{124}$Te. The subsequent measurements of the $g$-factor ratio, $g(^{124}\text{Te})/g(^{122}\text{Te})$, by the transient-field technique, clearly favor the conventional weighted average or LSW values over those given by the NRM and RT; evidently these latter averaging procedures should not be used for this data set.

According to the LSW procedure, the uncertainty in the average radioactivity $g$ factor for $^{122}$Te is $\sim\pm 9\%$, larger than that assigned to the conventional weighted average ($\sim\pm 5.5\%$). Because the LSW technique tends to reduce the contribution of the most statistically precise measurement in the data set and the focus here is on relative $g$ factors, the smaller error given by the conventional averaging procedure has been adopted. It should be noted, however, that the radioactivity measurements, which set the absolute scale of the $g$-factors reported below, could be uncertain by about 9%.

Calibration of the transient-field strength must use either the radioactivity measurements as normalization, or adopt one of the global parametrizations of the transient-field strength. Dunham *et al.* [9] and Thornton *et al.* [10] normalized their $g$ factors to the radioactivity results, while Shu *et al.* [8] employed the Rutgers parametrization [55] to calibrate the transient-field strength. These previous transient-field studies show reasonable consistency between the field strength predicted by the Rutgers parametrization and the experimental transient-field strengths extracted from the precession data for $^{122}$Te and $^{124}$Te using the radioactivity $g$ factors for calibration. In the previous measurements 80-MeV $^{32}$S and 70-MeV $^{35}$Cl beams were used with iron foils about 1.5 mg/cm$^2$ thick; the transient field was sampled at an average velocity of $\langle v/v_0\rangle \sim 3$. The Rutgers parametrization for ions in this region was determined largely by measurements on Pd ($Z = 46$) and Sm ions ($Z = 62$) traversing iron hosts with velocities below $3.5v_0$. The present experiment differs significantly in the use of a $^{58}$Ni beam to produce a much higher initial velocity for the Te ions, and a much thicker iron layer to increase the precession angle; the average velocity is higher and the velocity range is greater than in the previous studies. If the Rutgers parametrization were used to calibrate the present

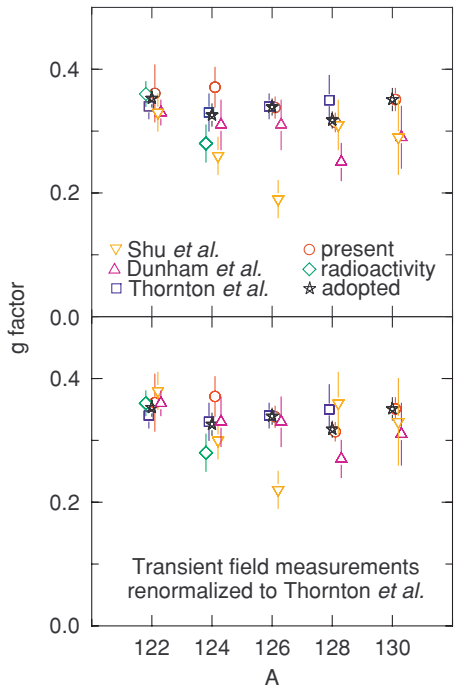


FIG. 5. (Color online) Comparison of transient field $g$-factor measurements and the average of the radioactivity results (see Fig. 4). The upper panel shows the transient field results as originally reported, however the different workers used different calibration procedures to obtain absolute $g$ factors. The lower panel shows the transient field results all renormalized to the measurements of Thornton *et al.* [10], which facilitates the comparison of the various measurements.

TABLE V. Comparison of experimental $g$ factors.

| Isotope | Values included in average | | | Average[a] | Other values | |
|---|---|---|---|---|---|---|
| | Radioactivity | Thornton *et al.* | Present | | Shu *et al.* | Dunham *et al.* |
| $^{122}$Te | 0.364(20) | 0.34(2) | 0.361(46) | 0.353(14) | 0.33(3) | 0.33(2) |
| $^{124}$Te | 0.277(32) | 0.33(3) | 0.371(32) | 0.326(18) | 0.26(3) | 0.31(4) |
| $^{126}$Te | | 0.34(2) | 0.338(17) | 0.339(13) | 0.19(3) | 0.31(4) |
| $^{128}$Te | | 0.35(4) | 0.314(15) | 0.318(13) | 0.31(5) | 0.25(3) |
| $^{130}$Te | | | 0.351(18) | 0.351(18) | 0.29(7) | 0.29(5) |

[a]Assigned errors reflect the uncertainties in the relative $g$ factors.

measurements, the precession per unit $g$ factor, Eq. (12), would be $\phi_{\text{Rutgers}}(\infty) = -81$ mrad, and the absolute $g$ factors would be about 20% smaller than in the previous studies. However a calibration of the high-velocity transient-field strength for Pd ($Z = 46$) in iron [60] is more closely matched to the present measurements on Te ions ($Z = 52$). Adopting the parametrization proposed in [60] to calibrate the present measurements would give $\phi_{\text{Pd}}(\infty) = -66$ mrad, and absolute $g$ factors for the Te isotopes in agreement with the previous work.

Rather than rely on one of the parametrizations, the present absolute $g$ factors were determined by normalizing the precession data to the $g$ factors of Thornton *et al.* [10]. These data were chosen to provide the normalization because Thornton *et al.* performed simultaneous relative measurements, like the present work, and normalized their results to the independently determined radioactivity results. As a result of this procedure, the experimental precession per unit $g$ factor is $\phi = -64 \pm 4$ mrad.

The present and previous $g$-factor results are compared in Fig. 5. In the upper panel the $g$ factors of Shu *et al.* and Dunham *et al.* are shown as reported by the authors. To help compare the relative $g$ factors obtained in the various transient-field studies, the lower panel shows these sequential transient-field measurements renormalized to the simultaneous measurements of Thornton *et al.* [10]. (In other words the differences due to the transient-field calibrations have been factored out so that no measurement is systematically higher or lower that any other measurement; equivalently, the average of the $g$ factors across the sequence of isotopes is the same for all four transient-field studies.) The level of consistency between the different measurements is then more apparent. Clearly, the low $g(2^+)$ value in $^{126}$Te reported by Shu *et al.* is not confirmed by the subsequent measurements, including the present work. This discrepancy is probably associated with systematic errors that are hard to control when transient-field measurements are performed sequentially, using a separate target for each isotope. Apart from the discrepant value for $^{126}$Te, the remaining measurements by Shu *et al.* and Dunham *et al.* appear to be in reasonable agreement with the other measurements. However, in view of the possibility for systematic errors, these sequential transient-field measurements were excluded from the average of the $g$ factors adopted for the analysis of the recoil in vacuum interaction [28]. For this purpose, the present work determines $g(^{130}\text{Te})/g(^{126}\text{Te})$ with much higher precision than the previous work; $g(^{122}\text{Te})/g(^{126}\text{Te})$ was already determined with sufficient precision by Thornton *et al.* [10]. The reasons for the selection of data included in the $g$ factors adopted for the RIV studies have been set out above. It might nevertheless be reasonable to include additional measurements from Table V in the adopted $g$ factors, however the impact on the analysis of RIV in [28] would be minor because the relevant $g$-factor ratios have now been determined precisely.

## V. EXPERIMENTAL RESULTS: $^{125}$Te

A summary of the $g$ factors measured in $^{125}$Te is given in Table VI. As for the even isotopes, the angular correlations were calculated. Where required, the multipolarity mixing ratios required were taken from Nuclear Data Sheets [62].

TABLE VI. Measured $g$ factors in $^{125}$Te.

| Level | | Transition | | | $\Delta\Theta$ (mrad) | $g(I_i^\pi)$ | |
|---|---|---|---|---|---|---|---|
| $E_x$ (keV) | $I_i^\pi$ | $E_\gamma$ (keV) | $I_i^\pi \to I_f^\pi$ | $\delta$[a] | | Present | Ref. [61] |
| 444 | $3/2_2^+$ | 408 | $3/2_2^+ \to 3/2_1^+$ | +1.50(7) | −33(12) | | |
| | | 444 | $3/2_2^+ \to 1/2_1^+$ | −2.3(1) | −84(26) | | |
| | | | | | ⟨−42(11)⟩[b] | +0.66(18) | +0.43(12) |
| 464 | $5/2_1^+$ | 428 | $5/2_1^+ \to 3/2_1^+$ | −0.538(11) | −26(6) | | |
| | | 464 | $5/2_1^+ \to 1/2_1^+$ | $\infty$ | −1(14) | | |
| | | | | | ⟨−21.5(56)⟩[b] | +0.34(9) | +0.20(5) |

[a]$E2/M1$ mixing ratios from [62].
[b]Weighted average.

The transient-field strength was calibrated as described for the even isotopes.

Table VI includes a comparison with the previous data [61]. Although the present experiments were not optimized to study $^{125}$Te, the measured $g$ factors have comparable precision to those reported previously. There is also a general similarity between the present and previous results concerning the precision and level of consistency between the precession angles measured for the alternative decays from the $3/2_2^+$ and $5/2_1^+$ states.

The present and previous [61] results agree within errors, however there may be a systematic difference in the absolute values. It should be noted that the present results for $^{125}$Te are normalized relative to the simultaneously measured even isotopes, whereas the transient-field strength in the previous measurement was calibrated using the Rutgers parametrization.

## VI. SUMMARY AND CONCLUDING REMARKS

Transient-field measurements have been performed for the $2_1^+$ states in the even isotopes $^{122,124,126,128,130}$Te and also for the $3/2_2^+$ (444 keV) and $5/2_1^+$ (464 keV) states in $^{125}$Te. The primary purpose was to determine the relative $g(2^+)$ values in $^{130}$Te and $^{126}$Te, to calibrate the radioactive beam measurements on $^{132}$Te and neighboring nuclei by the RIV technique. To eliminate potential sources of error, the $g$ factors were measured simultaneously, relative to each other. The precision has been improved compared with previous measurements by increasing the precession angles by a factor of $\sim$3. The application of the present results to the calibration of the RIV interaction for Te ions and the implications for $g$-factor measurements on radioactive beams, including $^{132}$Te, is discussed in an accompanying paper [28].

## ACKNOWLEDGMENTS

This work was motivated by the radioactive beam $g$-factor program at the Holified Radioactive Ion Beam Facility (HRIBF) at Oak Ridge National Laboratory and collaborative work with the authors of Ref. [7]. We are grateful to the technical staff of the Department of Nuclear Physics (Australian National University) for their support.

[1] D. C. Radford, C. Baktash, J. R. Beene, B. Fuentes, A. Galindo-Uribarri, C. J. Gross, P. A. Hausladen, T. A. Lewis, P. E. Mueller, E. Padilla *et al.*, Phys. Rev. Lett. **88**, 222501 (2002).
[2] C. J. Barton, M. A. Caprio, D. Shapira, N. V. Zamfir, D. S. Brenner, R. L. Gill, T. A. Lewis, J. R. Cooper, R. F. Casten, C. W. Beausang *et al.*, Phys. Lett. **B551**, 269 (2003).
[3] J. Terasaki, J. Engel, W. Nazarewicz, and M. Stoitsov, Phys. Rev. C **66**, 054313 (2002).
[4] N. Shimizu, T. Otsuka, T. Mizusaki, and M. Honma, Phys. Rev. C **70**, 054313 (2004).
[5] B. A. Brown, N. J. Stone, J. R. Stone, I. S. Towner, and M. Hjorth-Jensen, Phys. Rev. C **71**, 044317 (2005).
[6] G. Jakob, N. Benczer-Koller, G. Kumbartzki, J. Holden, T. J. Mertzimekis, K. H. Speidel, R. Ernst, A. E. Stuchbery, A. Pakou, P. Maier-Komor *et al.*, Phys. Rev. C **65**, 024316 (2002).
[7] N. J. Stone, A. E. Stuchbery, M. Danchev, J. Pavan, C. L. Timlin, C. Baktash, C. Barton, J. Beene, N. Benczer-Koller, C. R. Bingham *et al.*, Phys. Rev. Lett. **94**, 192501 (2005).
[8] N. K. B. Shu, R. Levy, N. Tsoupas, A. Lopez-Garcia, W. Andrejtscheff, and N. Benczer-Koller, Phys. Rev. C **24**, 954 (1981).
[9] J. S. Dunham, R. T. Westervelt, R. Avida, and S. S. Hanna, Phys. Rev. C **37**, 2881 (1988).
[10] J. L. Thornton, B. T. Neyer, and S. S. Hanna, Bull. Am. Phys. Soc. **30**, 1284 (1985).
[11] N. J. Stone, At. Data Nucl. Data Tables **90**, 75 (2005).
[12] J. Barrette, M. Barrette, R. Haroutunian, G. Lamoureux, and S. Monaro, Phys. Rev. C **10**, 1166 (1974).
[13] R. D. Larsen, W. R. Lutz, T. V. Ragland, and R. P. Scharenberg, Nucl. Phys. **A221**, 26 (1974).
[14] A. M. Kleinfeld, G. Mäggi, and D. Werdecker, Nucl. Phys. **A248**, 342 (1975).
[15] T. V. Ragland, R. J. Mitchell, and R. P. Scharenberg, Nucl. Phys. **A250**, 333 (1975).
[16] A. Bockisch and A. M. Kleinfeld, Nucl. Phys. **A261**, 498 (1976).
[17] M. J. Bechara, O. Dietzsch, M. Samuel, and U. Smilansky, Phys. Rev. C **17**, 628 (1978).
[18] R. R. Borchers, J. D. Bronson, L. Grodzins, R. Kalish, and D. E. Murnick, Phys. Rev. Lett. **17**, 1099 (1966).
[19] K. Johansson, E. Karlsson, and R. W. Sommerfeldt, Phys. Lett. **22**, 297 (1966).
[20] K. Auerback, B. Harns, K. Siepe, G. Wittkemper, and H. J. Horner, Phys. Lett. **22**, 299 (1966).
[21] S. K. Bhattacherjee, J. D. Bowman, and E. N. Knaufmann, Phys. Lett. **B24**, 65 (1967).
[22] J. Murray, T. A. McMath, and J. A. Cameron, Can. J. Phys. **45**, 1821 (1967).
[23] J. Murray, T. A. McMath, W. H. Brooker, and J. A. Cameron, Can. J. Phys. **45**, 1600 (1967).
[24] E. Bozck, R. Broda, J. Golezewski, A. Z. Hrynkiewicz, R. Kulessa, S. Ogaza, M. Rybicka, and W. Walus, in *Hyperfine Structure and Nuclear Radiation*, edited by E. Matthias and D. A. Shirley (North Holland, Amsterdam, 1968), p. 158.
[25] G. M. Heestand, R. R. Borchers, B. Herskind, L. Grodzins, R. Kalish, and D. E. Murnick, Nucl. Phys. **A133**, 310 (1969).
[26] G. K. Hubler, H. W. Kugel, and D. E. Murnick, Phys. Rev. C **9**, 1954 (1974).
[27] R. R. Borchers, B. Herskind, J. D. Bronson, L. Grodzins, R. Kalish, and D. E. Murnick, Phys. Rev. Lett. **20**, 424 (1968).
[28] A. E. Stuchbery and N. J. Stone Phys. Rev. C **76**, 034307 (2007).
[29] A. E. Stuchbery, I. Morrison, L. D. Wood, R. A. Bark, H. Yamada, and H. H. Bolotin, Nucl. Phys. **A435**, 635 (1985).
[30] A. P. Byrne, A. E. Stuchbery, H. H. Bolotin, C. E. Doran, and G. J. Lampard, Nucl. Phys. **A466**, 419 (1987).
[31] M. P. Robinson, A. E. Stuchbery, E. Bezakova, S. M. Mullins, and H. H. Bolotin, Nucl. Phys. **A647**, 175 (1999).
[32] E. Bezakova, A. E. Stuchbery, H. H. Bolotin, W. A. Seale, S. Kuyucak, and P. Van Isacker, Nucl. Phys. **A669**, 241 (2000).
[33] A. E. Stuchbery and E. Bezakova, Aust. J. Phys. **51**, 183 (1998).

[34] N. Benczer-Koller, M. Hass, and J. Sak, Annu. Rev. Nucl. Sci. **30**, 53 (1980).
[35] A. E. Stuchbery, A. N. Wilson, P. M. Davidson, and N. Benczer-Koller, Nucl. Instrum. Methods Phys. Res. B **252**, 230 (2006).
[36] A. E. Stuchbery, H. H. Bolotin, C. E. Doran, and A. P. Byrne, Z. Phys. A **322**, 287 (1985).
[37] A. E. Stuchbery, L. D. Wood, H. H. Bolotin, C. E. Doran, I. Morrison, A. P. Byrne, and G. J. Lampard, Nucl. Phys. **A486**, 374 (1988).
[38] A. E. Stuchbery, A. G. White, G. D. Dracoulis, K. J. Schiffer, and B. Fabricius, Z. Phys. A **338**, 135 (1991).
[39] A. E. Stuchbery, G. J. Lampard, and H. H. Bolotin, Nucl. Phys. **A528**, 447 (1991).
[40] G. J. Lampard, A. E. Stuchbery, and H. H. Bolotin, Nucl. Phys. **A536**, 397 (1992).
[41] A. E. Stuchbery, S. S. Anderssen, H. H. Bolotin, A. P. Byrne, G. D. Dracoulis, B. Fabricius, and T. Kibédi, Z. Phys. A **342**, 373 (1992).
[42] G. J. Lampard, A. E. Stuchbery, H. H. Bolotin, and S. Kuyucak, Nucl. Phys. **A568**, 617 (1994).
[43] A. E. Stuchbery, T. H. Heseltine, S. S. Anderssen, H. H. Bolotin, A. P. Byrne, B. Fabricius, and T. Kibédi, Hyperfine Interact. **88**, 97 (1994).
[44] A. E. Stuchbery and S. S. Anderssen, Phys. Rev. C **51**, 1017 (1995).
[45] S. S. Anderssen and A. E. Stuchbery, Hyperfine Interact. **96**, 1 (1995).
[46] S. S. Anderssen, A. E. Stuchbery, and S. Kuyucak, Nucl. Phys. **A593**, 212 (1995).
[47] A. E. Stuchbery, G. J. Lampard, and H. H. Bolotin, Nucl. Phys. **A642**, 361 (1998).
[48] A. E. Stuchbery, S. S. Anderssen, and H. H. Bolotin, Nucl. Phys. **A669**, 27 (2000).
[49] P. F. Mantica, A. E. Stuchbery, D. E. Groh, J. I. Prisciandaro, and M. P. Robinson, Phys. Rev. C **63**, 034312 (2001).
[50] A. E. Stuchbery and M. P. Robinson, Nucl. Instrum. Methods Phys. Res. A **485**, 753 (2002).
[51] K. Alder and A. Winther, *Electromagnetic Excitation* (North-Holland, Amsterdam, 1975).
[52] T. Yamazaki, Nucl. Data A **3**, 1 (1967).
[53] A. Winther and J. de Boer, in *Coulomb Excitation*, edited by K. Alder and A. Winther (Academic Press, New York, 1966), p. 303.
[54] J. F. Ziegler, J. P. Biersack, and U. Littmark, *The Stopping and Range of Ions in Solids*, Vol. 1 of *The Stopping and Ranges of Ions in Matter*, edited by J. F. Ziegler (Permagon, New York, 1985).
[55] N. K. B. Shu, D. Melnik, J. M. Brennan, W. Semmler, and N. Benczer-Koller, Phys. Rev. C **21**, 1828 (1980).
[56] A. E. Stuchbery, A. D. Davies, P. F. Mantica, P. M. Davidson, A. N. Wilson, A. Becerril, B. A. Brown, C. M. Campbell, J. M. Cook, D. C. Dinca *et al.*, Phys. Rev. C **74**, 054307 (2006).
[57] A. E. Stuchbery and E. Bezakova, Phys. Rev. Lett. **82**, 3637 (1999).
[58] S. Raman, C. W. Nestor, and P. Tikkanen, At. Data Nucl. Data Tables **78**, 1 (2001).
[59] M. U. Rajput and T. D. Mac Mahon, Nucl. Instrum. Methods Phys. Res. A **312**, 289 (1992).
[60] A. E. Stuchbery, C. G. Ryan, H. H. Bolotin, and S. H. Sie, Phys. Rev. C **23**, 1618 (1981).
[61] N. Benczer-Koller, G. Lenner, R. Tanczyn, A. Pakou, G. Kumbartzki, A. Piqué, D. Barker, D. Berdichevsky, and L. Zamick, Phys. Rev. C **40**, 77 (1989).
[62] J. Katakura, Nucl. Data Sheets **86**, 955 (1999).